Article

Unmasking Intra-Tumoral Heterogeneity and Clonal Evolution in NF1-MPNST

Chang-In Moon [1,†], William Tompkins [2,†], Yuxi Wang [1], Abigail Godec [3], Xiaochun Zhang [1], Patrik Pipkorn [4,5] , Christopher A. Miller [5,6], Carina Dehner [7], Sonika Dahiya [5,7] and Angela C. Hirbe [1,5,*]

[1] Division of Medical Oncology, Department of Medicine, Washington University School of Medicine, St. Louis, MO 63110, USA; moonchangin@wustl.edu (C.-I.M.); yuxi.w@wustl.edu (Y.W.); zhang.x@wustl.edu (X.Z.)

[2] Washington University School of Medicine, St. Louis, MO 63110, USA; wtompkins@wustl.edu

[3] College of Human Medicine, Michigan State University, East Lansing, MI 48824, USA; godecabi@msu.edu

[4] Department of Otolaryngology, Division of Head and Neck Surgery, Washington University School of Medicine, St. Louis, MO 63110, USA; ppipkorn@wustl.edu

[5] Siteman Cancer Center, St. Louis, MO 63110, USA; c.a.miller@wustl.edu (C.A.M.); sdahiya@wustl.edu (S.D.)

[6] McDonnell Genome Institute, Division of Oncology—Stem Cell Biology, Department of Medicine, Washington University School of Medicine, St. Louis, MO 63110, USA

[7] Department of Pathology and Immunology, Washington University School of Medicine, St. Louis, MO 63110, USA; cdehner@wustl.edu

* Correspondence: hirbea@wustl.edu; Tel.: +1-314-747-3096

† These authors contributed equally.

check for updates

Abstract: Sarcomas are highly aggressive cancers that have a high propensity for metastasis, fail to respond to conventional therapies, and carry a poor 5-year survival rate. This is particularly true for patients with neurofibromatosis type 1 (NF1), in which 8%–13% of affected individuals will develop a malignant peripheral nerve sheath tumor (MPNST). Despite continued research, no effective therapies have emerged from recent clinical trials based on preclinical work. One explanation for these failures could be the lack of attention to intra-tumoral heterogeneity. Prior studies have relied on a single sample from these tumors, which may not be representative of all subclones present within the tumor. In the current study, samples were taken from three distinct areas within a single tumor from a patient with an NF1-MPNST. Whole exome sequencing, RNA sequencing, and copy number analysis were performed on each sample. A blood sample was obtained as a germline DNA control. Distinct mutational signatures were identified in different areas of the tumor as well as significant differences in gene expression among the spatially distinct areas, leading to an understanding of the clonal evolution within this patient. These data suggest that multi-regional sampling may be important for driver gene identification and biomarker development in the future.

Keywords: NF1; MPNST; genomics; heterogeneity

1. Introduction

Malignant peripheral nerve sheath tumor (MPNSTs) is the sixth most common soft tissue sarcoma [1] and has an incidence rate of 0.1–0.2 per 100,000 persons per year [2]. MPNSTs are often associated with neurofibromatosis type 1 (NF1). The incidence rate of MPNSTs in patients with NF1 is much higher than that of the general population, estimated to be 1.6 per 1000 per year, or a lifetime risk of 8–13% [3]. Approximately 50% of MPNSTs occur in patients with neurofibromatosis [4–7], and the other 50% of MPNSTs occur sporadically or in the setting of previous radiation therapy [4,6].

In the setting of NF1, MPNSTs often arise within a pre-existing benign nerve sheath tumor (plexiform neurofibroma) [4,7].

Prognosis remains poor for patients with MPNST despite multi-modality therapy [2,5–10]. In the setting of metastatic disease, treatment is limited to cytotoxic chemotherapy, typically consisting of single agent doxorubicin or a combination of doxorubicin and ifosfamide [11–13].

A number of different genes have been implicated in the development of MPNSTs. One of the most commonly used models for preclinical testing was developed by Cichowski et al. and Vogel et al; they demonstrated that mice with germline variants in *Nf1* and *Tp53* develop MPNSTs, supporting a cooperative and causal role for these tumor suppressors in the context of MPNST formation [14,15]. Other groups have found a reduction in expression of *PTEN*, a tumor suppressor in the *PI3K/AKT/mTOR* pathway, in MPNSTs compared to benign nerve sheath tumors in a manner that is not regulated by *NF1* [16]. Keng et al. went on to demonstrate the cooperative roles of *Pten* and *Nf1* in the tumorigenesis of MPNSTs in vivo with transgenic mouse models [17]. Gregorian et al. further elucidated the cooperative relationship between *k-ras* activation and *Pten* deletion, showing that both variants in combination led to 100% penetrable development of MPNSTs [18]. Another gene implicated in MPNST pathogenesis is *INK4A*, a tumor suppressor encoding both *p16* and *p19*. Deletions in this gene have been identified in MPNSTs but not in benign neurofibromas [19]. Lu et al. demonstrated a difference in aberrant expression of *ATRX*, a DNA helicase that plays a role in chromatin regulation and maintenance of telomeres, between MPNSTs and benign neurofibromas [20]. Additionally, variants in *EED* and *SUZ12* have been observed in MPNST. These genes code for components of the PRC2 complex which is involved in transcriptional repression. Lee et al. showed loss-of-function somatic alterations of PRC2 components in 92% of sporadic, 70% of NF1-associated and 90% of radiotherapy-associated MPNSTs. Further, introduction of the lost PRC2 component in a PRC2-deficient MPNST cell line decreased cell growth [21]. Others have found alterations such as structural alterations of *PDGFRA* (platelet-derived growth factor-α) in 26% of MPNST samples [22]; increased expression of *EGF-R* (epidermal growth factor receptor) by immunohistochemistry in MPNSTs [23]; and *IGFR1* gene amplification in 24% of MPNSTs [24].

Despite all of this research, no effective therapies have emerged from recent clinical studies based on this genomic data and subsequent preclinical studies. Intra-tumoral heterogeneity is a possible reason for these shortcomings. Prior studies have relied on a single sample from these tumors. All the subclones within a tumor may not be captured by this approach. Our aim in this study is to investigate intra-tumoral heterogeneity more thoroughly through analysis of samples taken from multiple sites of the same MPNST.

2. Materials and Methods

2.1. Study Approvals

Blood and tumor were obtained from an individual diagnosed with NF1 according to established criteria [25] and treated for a MPNST at Washington University/St. Louis Children's Hospital NF Clinical Program (St. Louis, MO, USA). The human tumor samples were collected under an approved IRB protocol (#201203042) at Washington University, and the patient was appropriately consented.

2.2. Sample Collection

Samples were taken from three distinct areas within a single tumor from a patient with an NF1-MPNST immediately after surgical resection with guidance from a pathologist (SD). While area "1" represented solid, tan homogeneous tumor lacking hemorrhage and/or necrosis, areas "2" and "3" of the tumor grossly appeared necrotic and hemorrhagic respectively. 20 g of tissue was taken from each area. Each area was then divided to be used for RNA extraction, DNA extraction, and slide preparation to analyze the histology. A gross image of the tumor was taken at this time and is shown as Figure 1.
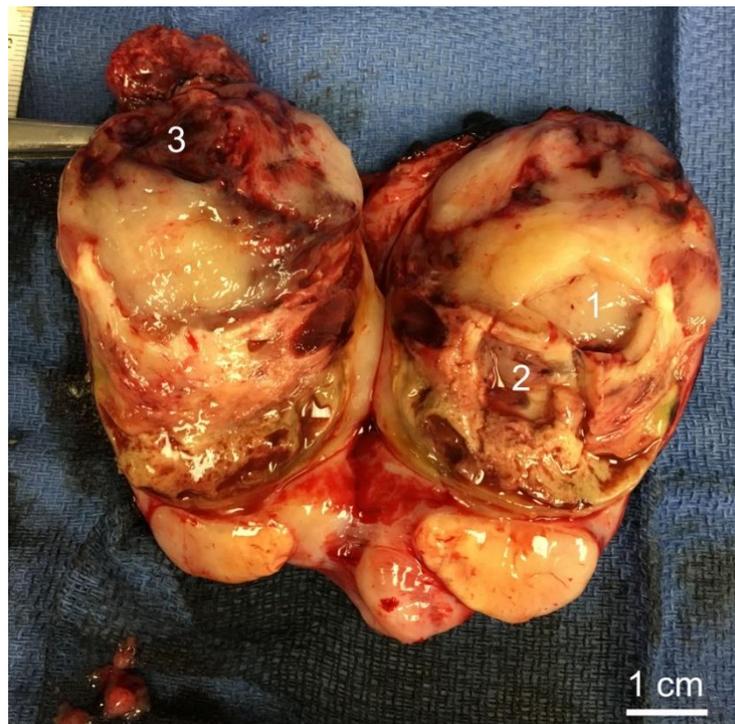
Figure 1. Malignant peripheral nerve sheath tumor (MPNST) sampled areas. Area 1 shows an area centrally located in MPNST, Area 2 an area of hemorrhage, and Area 3 an area of necrosis.

2.3. Histology

Images of the hematoxylin-eosin sections were taken (20X magnification) using an Olympus BX-51 microscope using an Olympus DP71 digital camera, and DP Controller software. Tumor purity was estimated based on morphologic review of the entire hematoxylin-eosin stained section estimating the number of tumor cells, stromal cells, lymphocytes, and extravasated red blood cells. Two pathologists reviewed these slides independently providing an estimated percentage of total tumors cells per slide.

2.4. Sequencing and Bioinformatics Analysis

Whole exome sequencing (WES), RNA sequencing (RNA-Seq), and copy number analysis (CNVkit) [26] were performed on each sample and compared to a blood sample as a germline DNA control. Both Illumina Whole Genome Sequencing (eWGS) of 3 tumor samples and 1 PBMC normal sample, and Illumina RNA Sequencing of the 3 tumor samples were generated from the sampled areas.

2.4.1. Library Construction and Sequencing

Each tumor had 2 enriched libraries constructed (n = 6), and the PBMCs had a single enriched library constructed (n = 1). Exome libraries were captured with an IDT exome reagent, then pooled with a WGS library for sequencing on an Illumina HiSeq4000 with at least 1000x coverage. RNA was prepared with a TrueSeq stranded total RNA library kit, then sequenced on an Illumina HISeq4000 with 72M reads per sample.

2.4.2. IDT Exome Sequencing Variant Detection

Genomic data were aligned against reference sequence hg38 via BWA-MEM [27] with Base Quality Score Recalibration (BQSR). Structural variants (SVs) and large indels were detected using manta [28]. SNVs and small indels were detected using VarScan2 [29], Strelka2 [30], MuTect2 [31], and Pindel [32] via the somatic pipelines available at https://github.com/genome/analysis-workflows, which includes best-practice variant filtering and annotation with VEP (Variant Effect Predictor, version 95) [33].

Manual review was used to remove additional sequencing artifacts. Germline variants and somatic variants reported on variant detecting pipeline were compared to see any intersection of variants. Any intersecting variants were removed from the somatic variant gene list, thus filtering out the germline variants. Common variants with 1000 genome MAF (minor allele frequency) > 0.05 were filtered out. Waterfall somatic variant plots were created with GenVisR [34] by including somatic variants that occurred in each area. Variants reported on the waterfall plot are most likely to be pathogenic, which is reported via VEP. These variants were not reported as a somatic variant in COSMIC (Catalogue Of Somatic Mutations In Cancer) [35] and ClinVar [36] archive, thus these variants are best classified as variants with unknown significance. In order to predict clinical significance and predictions of the functional effects of these variants, each variant was reviewed on SIFT [37] and Polyphen [38]. IMPACT rating was determined by VEP for each non-coding variant.

2.4.3. Copy Number Analysis

CNVkit was used to infer and visualize copy number from high-throughput DNA sequencing data. Coverage for each bait position in the exome reagent was calculated, then segments of constant copy number were identified using circular binary segmentation. Data were plotted to provide visualization of CNVs.

2.4.4. Inference of Clonal Phylogeny

SciClone [39] and ClonEvol [40] were utilized to attempt to perform a phylogeny inference. However, the analysis was complicated by the abundance of copy number-altered regions in these tumors, and these standard algorithms were unable to automatically perform that inference. Manual review of the shared and private single nucleotide variants and large copy number altered areas, though, revealed only one possible phylogeny for this tumor.

2.4.5. RNA Sequence Preprocessing

RNA-Sequence (RNA-seq) was trimmed from 3'-end with a minimum quality Phred score of 20 and aligned against hg38—Ensembl Transcripts release 99 via BWA-MEM. Pre/post quality control and full expectation-maximization (EM) quantification were run via Partek$^®$ Flow$^®$ [41]. Gene counts and transcript counts were normalized by CPM (counts per million) by using edgeR [42] package. Heatmap visualizations were created using gplots [43] R package (Warnes, G.R. Seattle, WA, USA).

2.4.6. Gene Differential Expression Analysis

The gene-specific analysis (GSA) method was used to test for differential expression of genes or transcript between sample regions in Partek$^®$ Flow$^®$ [44]. Differential expressed genes were defined as the following statistic parameters: p-value <= 0.05; FDR step up <= 0.05; Fold Change < −2 or >2. From differentially expressed genes, a GO enrichment test was used to functionally profile this set of genes, to determine which GO terms appear more frequently than would be expected by chance when examining the set of terms annotated to the input genes, each associated with a p-value.

2.4.7. Pathway Analysis

A list of genes in copy number aberrant (CNA) regions was extracted. CNA regions were defined as copy number regions greater than 3 or copy number regions less than 1. For each area, we intersected the list of genes that are located in the CNA regions with the differentially expressed gene list reported in the RNA differential expression analysis (p-value <= 0.05). PantherDB [45] was utilized to discover GO terms and pathways that may be affected by these genes.

3. Results

3.1. Patient Information

Patient characteristics can be seen in Table 1. The patient was a male with a history significant for a clinical diagnosis of neurofibromatosis type 1—patient had a plexiform neurofibroma, spinal neurofibromas, café au lait macules, and multiple first-degree relatives with neurofibromatosis type 1—and was 40 years old at the time of diagnosis of MPNST. He presented with a large tumor located in the left neck. Resection showed a high-grade malignant peripheral nerve sheath tumor, 10.2 cm in the largest dimension, with negative margins. The patient did not receive any adjuvant therapy for his MPNST following initial resection due to poor performance status. He recurred 21 months after the initial diagnosis and ultimately died secondary to complications from metastatic disease (33 months after initial diagnosis). Samples were taken in three different locations within the primary tumor immediately following the initial resection for the purpose of this study.

Table 1. Patient Characteristics.

Age at Diagnosis, Years	Sex	Tumor Location	Tumor Size/Grade	Surgical Margin Status	Disease Status	Metastasis	Adjuvant Treatment	OS *, Months
40	Male	Left neck	10.2 cm, Grade 3 [1]	Negative	Recurred	Lung	None	33

[1] By French Federation of Cancer Centers Sarcoma Group Grading System (FNCLCC) [46]; * OS = Overall Survival-time from diagnosis of MPNST to death.

3.2. Histology of Biopsy Sites

We first reviewed the H&E images of the tumor to correlate histology to the gross images of the tumor. H&E stained sections in Figure 2 show representative images of the three sampled areas. Area #1 demonstrates tissue of a spindle cell neoplasm of neural differentiation arranged in fascicles with elongated hyperchromatic nuclei and a mild to moderate amount of cytoplasm. The tumor purity of this sample was >95%. Area #2 shows spindled cells in a background of hemorrhage, a finding commonly seen in these high-grade tumors with a tumor purity of >95%. Area #3 represents an area of necrosis, another characteristic finding for MPNST. This sample showed >95% tumor purity.
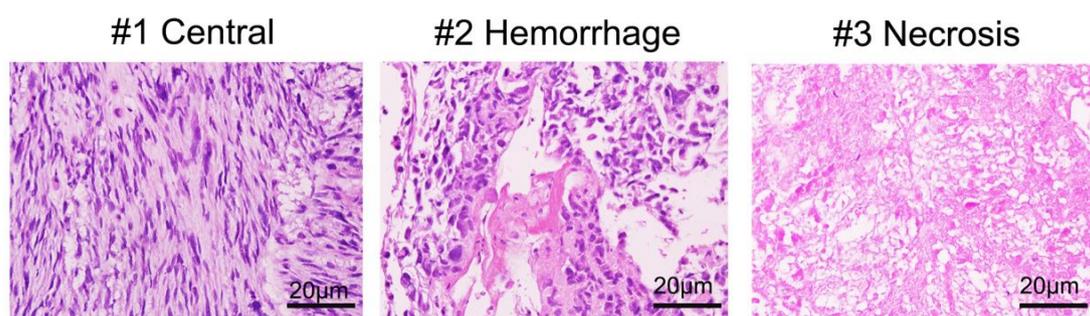
Figure 2. H&E stained sections of the biopsy sites. H&E stained sections (20X) show areas (#1) of relatively uniform, spindled cells with fascicular growth pattern, characteristic for MPNST. Sampled area #2 shows evidence of hemorrhage within the tumor, a feature commonly seen in MPNST. Area #3 shows abundant tumor necrosis.

3.3. Whole Exome Sequencing (WES), RNA Sequencing (RNA-Seq), and Copy Number Analysis

We first interrogated the sequencing data to identify the germline NF1 variant within this tumor. Figure 3 shows a lollipop plot identifying the patient's likely NF1 germline variant based on exclusion of any variants with minor allele frequency >0.05 in the 1000 genomes database. Next, to

investigate intra-tumoral heterogeneity within the sample, RNA sequencing of the three sample sites was performed and is shown in Figure 4.
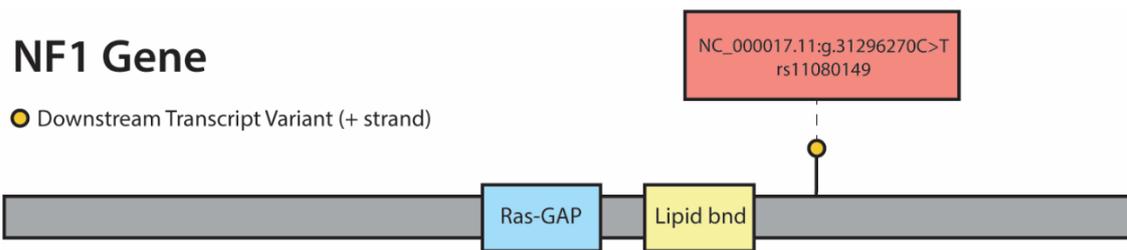
Figure 3. Location of NF1 germline variant. One intronic germline variant, NC_000017.11:g.31296270C>T (rs11080149). was identified and is depicted in this figure.
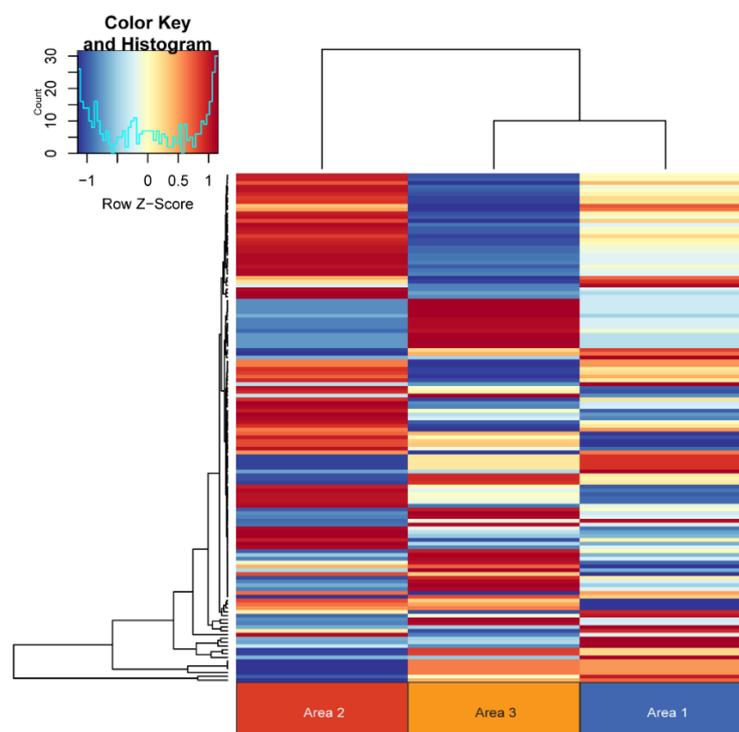
Figure 4. RNA-Seq Heatmap. Normalized read counts by counts per million (CPM) in differentially expressed genes are depicted here. Distinct gene expression profiles can be appreciated in each biopsied area. Each column is depicted as list of genes.

Distinct gene expression profiles were observed in each of the areas sampled. The top 16 differentially expressed genes are listed in Table 2 and include a number of genes involved in transcription and translation. We next performed a copy number analysis of the three biopsy sites to determine whether or not different copy number alterations were observed in each area (Figure 5). Distinct copy number signatures can be appreciated in each of the three samples further illustrating intra-tumoral heterogeneity. Additionally, we evaluated the single nucleotide variants found in each of the samples. This broad overview of all somatic variants is depicted in the waterfall plot in Figure 6. Again, distinct somatic variants can be appreciated across different areas. We next explored the potential significance of these variants through further bioinformatics analysis. While the biological significance of each of these variants is uncertain, there is evidence that some of these variants may play a role in the pathogenesis. For each variant in a coding region, CBioPortal [47] was queried for each gene to determine if the somatic variant was in a functional domain. Additionally, the RNAseq data was queried to determine if the variant in a specific area of the tumor influenced the gene expression of

that gene in a specific area. Finally, SIFT and Polyphen were used to predict pathogenicity. Table 3a,b list the somatic variants in the coding region that may play a role in the pathogenesis of this tumor based on the above criteria. For those mutaions in non-coding regions, the Ensembl Variant Effect Predictor [33] was used to determine whether or not the variant would be predicted to affect gene expression. All of the identified variants were classified as modifiers, indicating that pathogenicity prediction is difficult, thus the effects of these variants are unclear. (Table 3c). Further details of the somatic variants can be found in Supplemental Table S1. Next, a gene ontology analysis was performed. To do this, a list of genes in copy number aberrant (CNA) regions was extracted. For each area, the list of genes located in the CNA regions intersected with the differentially expressed gene list reported in the RNA differential expression analysis, and PantherDB [45] was utilized to identify pathways that may be affected by these genes. Table 4 displays the unique genes in each area with copy number aberrations and alterations in gene expression. Genes depicted in Area 1 have been reported in the literature to serve a myriad of functions in tumorigenesis, including base excision repair, nucleotide excision repair, and alternative splicing [48–55]. Those in Area 2 are involved in several different pathways, including transcriptional regulation in addition to ribosomal and proteasomal function [56–60]. Finally, the genes in Area 3 consist of several ribosomal subunits and small nucleolar RNAs, suggesting that both translation and transcription are uniquely affected compared to other areas [61–63]. This analysis suggests that there may be different functional programs at play across the three areas. Next, we manually reviewed the data to look for changes in other known drivers of MPNST including TP53, ATRX, EED, SUZ12, and CDKN2A. There were no copy number changes or somatic mutions in any of these genes. Finally, we performed a careful manual review of all of the shared and unique somatic variants and copy number alterations in each area in order to develop a predicted clonal evolution. Figure 7 depicts the predicted phylogenetic tree of the subclones from each area, representing the likely clonal evolution of the tumor.

Table 2. Top Differentially Expressed Genes. The gene-specific analysis was used to test for differential expression of genes or transcript between sample regions in Partek® Flow®. Statistical cutoff are made by these following parameters: *p*-value <= 0.05; FDR step up <= 0.05; Fold Change <−2 or >2.

Gene Symbol	*p*-Value (1 vs. 2)	Fold Change (1 vs. 2)	*p*-Value (1 vs. 3)	Fold Change (1 vs. 3)	*p*-Value (2 vs. 3)	Fold Change (2 vs. 3)
EEF1A1	2.04×10^{-84}	−3.32	3.33×10^{-16}	2.20	1.35×10^{-119}	7.31
RPS27	4.32×10^{-24}	−2.51	7.64×10^{-13}	3.01	4.27×10^{-46}	7.55
RPS27A	1.69×10^{-12}	−2.62	9.42×10^{-05}	2.27	4.16×10^{-21}	5.95
H3C3	7.46×10^{-12}	−4.51	5.05×10^{-04}	11.2	5.54×10^{-09}	50.6
RPLP1	2.36×10^{-10}	−2.57	7.25×10^{-04}	2.13	2.43×10^{-17}	5.48
SNORD13	3.24×10^{-10}	3.00	8.25×10^{-62}	−4.91	3.52×10^{-66}	−14.8
RPLP0	1.05×10^{-09}	−2.26	1.60×10^{-04}	2.09	1.73×10^{-18}	4.72
TPI1	1.65×10^{-08}	−2.27	5.61×10^{-04}	2.08	6.52×10^{-16}	4.72
RPL23AP42	3.77×10^{-07}	−2.21	8.40×10^{-04}	2.16	8.65×10^{-14}	4.78
RPS23	5.34×10^{-06}	−2.46	1.17×10^{-03}	2.92	9.16×10^{-11}	7.19
MT-TI	4.64×10^{-05}	3.44	1.19×10^{-15}	−3.67	6.36×10^{-20}	−12.6
SNORA81	2.28×10^{-04}	33.3	4.00×10^{-11}	−3.39	5.12×10^{-07}	−11.3
RNY1	2.45×10^{-04}	2.65	4.67×10^{-24}	−4.71	8.10×10^{-27}	−12.5
RNVU1-31	5.00×10^{-04}	−4.18	3.83×10^{-14}	−17.7	7.07×10^{-13}	−4.23
MT-TM	6.37×10^{-04}	3.70	2.29×10^{-07}	−2.89	2.69×10^{-11}	−10.7
TMSB4XP6	1.16×10^{-03}	3.19	2.89×10^{-04}	−2.15	7.91×10^{-09}	−6.87
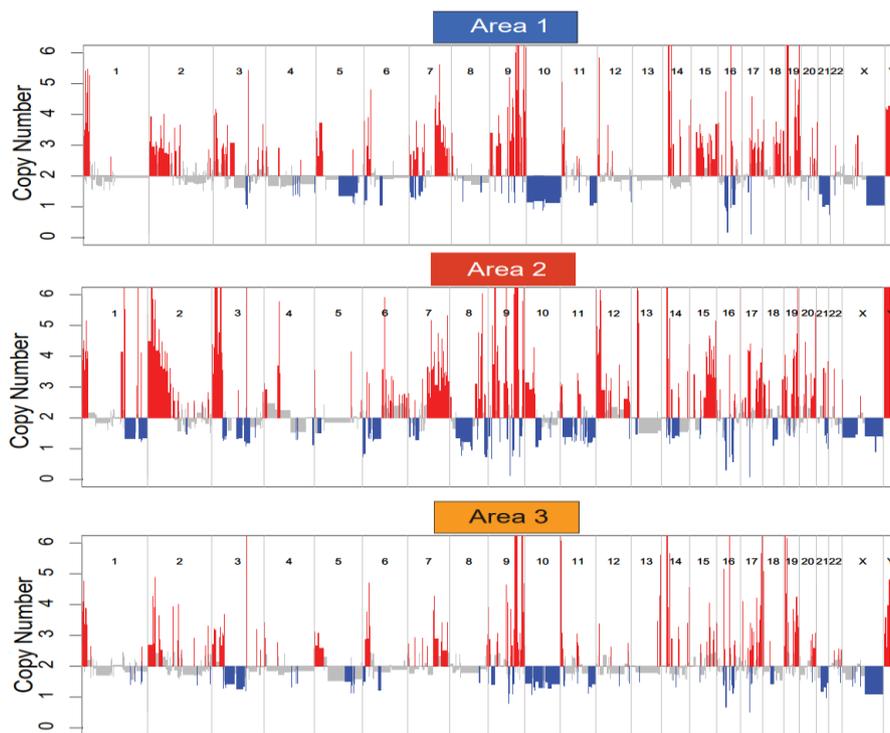
Figure 5. Copy Number Variation Plot. Copy number variation plots for each biopsied site demonstrate distinct copy number signatures.
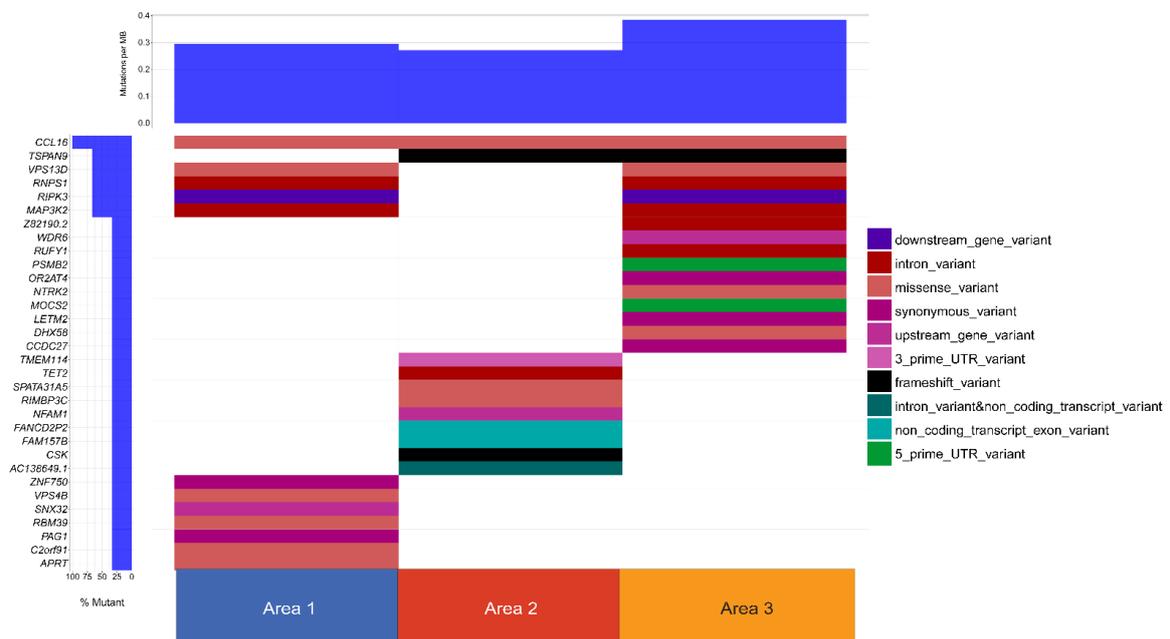
Figure 6. Somatic Variant Waterfall Plot. All somatic variants displayed on a waterfall plot. Each row represents a gene. Distinct somatic variant signatures are appreciated.

Table 3. (a) Details of the Tumor Related Somatic Variants in Coding Regions. Each gene with a somatic point variant is listed along with the area in which the variant occurred, the type of variant, the amino acid change, and whether or not the variant occurs in a putative functional domain. The final column lists whether or not the gene expression is altered in the area in which the variant occurred. The magnitude of gene expression is expressed as any of the following: NA indicates no change; "-" indicates 1-2 fold decrease in gene expression; "- -" indicates greater than 2 fold decrease in gene expression; "+" indicates 1-2 fold increase in gene expression; "+ +" indicates greater than 2 fold increase in gene expression compared to two other areas. Pathogenicity predictions are made based on SIFT and PolyPhen scores. (b) Details of the Tumor Related Somatic Frameshift Variants in Coding Regions. Each gene with a somatic point variant resulting in a frameshift is listed along with the area in which the frameshift variant occurred and whether or not the frameshift variant occurs in a putative functional domain. (c) Details of the Tumor Related Somatic Variants in Non-coding Transcript Exons, Untranslated Regions, Introns, and Upstream and Downstream Genes. Each gene with a somatic point variant is listed along with the area in which the variant occurred, the genomic location, the type of variant, and whether or not the gene expression is altered in the area in which the variant occurred. The magnitude of gene expression is expressed as: NA indicates no change; "-" indicates 1-2 fold decrease in gene expression; "- -" indicates greater than 2 fold decrease in gene expression; "+" indicates 1-2 fold increase in gene expression; "+ +" indicates greater than 2 fold increase in gene expression compared to two other areas. The final column lists the potential impact rating as evaluated by VEP. All of these variants are listed as "modifier" indicating that predictions are difficult or there is no evidence of impact.

(a)

Gene	Area	Genomic Location	Variant	Amino Acid Change	Functional Domain Affected	Gene Expression Altered	Pathogenicity Prediction
C2orf91	1	Chr2:41953024	missense	p.(Arg91Ile)	N	NA	Possibly damaging
CCL16	1	Chr17:35978161	missense	p.(Cys60Ser)	Y	NA	Probably damaging
PAG1	1	Chr8:80984896	synonymous	p.(Pro252=)	Y	NA	Unknown
VPS13D	1	Chr1:12283596	missense	p.(Phe1832Val)	N	-	Probably damaging
VPS4B	1	Chr18:63400074	missense	p.(Lys255Thr)	Y	NA	Probably damaging
ZNF750	1	Chr17:82830337	synonymous	p.(Pro659=)	N	NA	Unknown
RIMBP3C	2	Chr22:21546513	missense	p.(Arg1488Ser)	N	NA	Possibly Damaging
SPATA31A5	2	Chr9:60919364	missense	p.(Leu970Phe)	N	-	Possibly Damaging
CCDC27	3	Chr1:3752496	synonymous	p.(Ile5=)	N	+	Unknown
LETM2	3	Chr8:38400906	synonymous	p.(Leu279=)	Y	+	Unknown
NTRK2	3	Chr9:84670796	missense	p.(Trp16Cys)	N	NA	Possibly Damaging

(b)

Gene	Area	Genomic Location	Variant	Amino Acid Change	Functional Domain Affected
CSK	2	Chr15:74798671	frameshift	p.(Glu25fs)	Y
TSPAN9	2	Chr12:3283047	frameshift	p.(Leu218fs)	Y

Table 3. *Cont.*

(c)

Gene	Area	Genomic Location	Variant	Gene Expression Altered	IMPACT
MAP3K2	1	Chr2:127387525	intron	-	Modifier
RIPK3	1	Chr14:24332669 or Chr14:24332869	downstream gene	+	Modifier
RNPS1	1	Chr16:2266329	intron	-	Modifier
SNX32	1	Chr11:65832561	upstream gene	-	Modifier
AC138649.1	2	Chr15:22768761	intron	NA	Modifier
FAM157B	2	Chr9:138231054	non-coding transcript exon	+	Modifier
FANCD2P2	2	Chr3:11871392	non-coding transcript exon	+	Modifier
LAIR1	2	Chr19:54358582	intron	NA	Modifier
NFAM1	2	Chr22:42432412	upstream gene	+	Modifier
TET2	2	Chr4:105241954	intron	NA	Modifier
TMEM114	2	Chr16:8569715	3 prime UTR	NA	Modifier
MOCS2	3	Chr5:53109455	5 prime UTR	-	Unknown
PSMB2	3	Chr1:35641574	5 prime UTR	NA	Modifier
RUFY1	3	Chr5:179608552	intron	-	Modifier
WDR6	3	Chr3:49005134	upstream gene	NA	Modifier
Z82190.2	3	Chr22:31821630	intron	NA	Modifier

Table 4. Differentially Expressed Gene Pathway Analysis. These genes were located in copy number aberrant regions defined as copy number more than 3 or lower 1 and also demonstrated differential expression by RNA seq. Different pathways are implicated in the distinct sections.

Location	Chromosome	Start Position	End Position	Raw Copy Number	Genes	Role in Tumorigenesis
Area1	chr17	81509970	81523847	3.151914	ACTG1	Anti-apoptosis, motility [64,65]
Area1	chr17	81887843	81891586	3.151914	ALYREF	Genomic stability [66]
Area1	chr14	20455190	20457772	4.883921	APEX1	Base-excision repair [49]
Area1	chr17	81867720	81871406	3.151914	ARHGDIA	Invasiveness, metastasis [67]
Area1	chr12	7080208	7092607	5.842557	C1R	Inflammation [68]
Area1	chr17	79778131	79787983	3.109085	CBX2	Transcription [69]
Area1	chr17	50183288	50201632	3.060268	COL1A1	Metastasis [70]
Area1	chr17	82078332	82098332	3.562293	FASN	Metabolism [71]
Area1	chr7	128830376	128859274	3.66148	FLNC	Invasiveness [72]
Area1	chr17	82050690	82057470	3.562293	GPS1	COP9 signalosome subunit/ubiquitin-proteasome pathway
Area1	chr19	11164266	11197791	7.563794	KANK2	Cytoskeleton formation [73]
Area1	chrX	54807598	54816012	3.320925	MAGED2	Cell-cycle regulator [74]
Area1	chrX	55452104	55453566	3.320925	MAGEH1	Proliferation [75]
Area1	chr7	100092727	100101940	4.16605	MCM7	Proliferation [76]
Area1	chr14	22836556	22849027	4.136412	MMP14	Invasiveness, metastasis [77]
Area1	chr14	39175182	39183218	3.038443	PNN	Splicing [51]
Area1	chr9	107283136	107332194	14.61502	RAD23B	Nucleotide-excision repair [53]
Area1	chr18	49488452	49492523	3.095593	RPL17	Ribosome biogenesis, protein translation [61]
Area1	chrX	54814369	54814497	3.320925	SNORA11	Maturation of ribosomal RNA [62]
Area1	chr7	102194075	102194164	4.159154	SNORA48	Maturation of ribosomal RNA
Area1	chr2	5692666	5701385	3.929294	SOX11	Transcription
Area1	chr17	76734114	76737374	3.109085	SRSF2	Splicing [54]
Area1	chr9	35099775	35103195	3.374564	STOML2	Anti-apoptosis [78]
Area1	chr17	61399895	61409466	3.52571	TBX2	Transcription [79]
Area1	chr19	58544090	58550722	3.012426	TRIM28	Proliferation [80]
Area1	chr9	35056063	35073249	3.374564	VCP	Protein degradation [81]
Area1	chr7	101162508	101165593	4.159154	VGF	Transcription [82]
Area2	chr2	47335314	47335514	4.114423	BCYRN1	Transcription [56]
Area2	chr6	73515749	73523797	3.582945	EEF1A1	Translation [57]
Area2	chr19	3976055	3985469	3.359182	EEF2	Translation [58]
Area2	chr1	150574550	150579738	4.140715	MCL1	Anti-apoptosis [83]
Area2	chr1	151399533	151401944	4.140715	PSMB4	Proteasomal function [59]
Area2	chr11	67583594	67586660	3.211531	GSTP1	Metabolism [84]
Area2	chr15	65296050	65296166	3.976034	RNU5A-1	RNA processing
Area2	chr15	65304676	65304792	3.976034	RNU5B-1	RNA processing
Area2	chr7	148983754	148983856	3.383375	RNY3	RNA processing
Area2	chr13	27251308	27256691	6.141368	RPL21	Ribosome biogenesis, protein translation
Area2	chr9	19375714	19380254	3.739665	RPS6	Ribosome biogenesis, protein translation
Area2	chr2	24273613	24273741	4.326829	SCARNA21	RNA processing

Table 4. *Cont.*

Location	Chromosome	Start Position	End Position	Raw Copy Number	Genes	Role in Tumorigenesis
Area2	chr15	78091171	78091297	3.898802	SNORA63	Maturation of ribosomal RNA
Area2	chr1	12221147	12221271	3.552826	SNORA70	Maturation of ribosomal RNA
Area2	chr2	10446713	10446849	4.496897	SNORA80B	Maturation of ribosomal RNA
Area2	chr12	124911603	124917368	3.034233	UBC	Ubiquitin homeostasis [85]
Area3	chr16	28823034	28837237	5.159031	ATXN2L	Stress granule regulator [86]
Area3	chr9	136862118	136866286	3.830137	EDF1	Transcription
Area3	chr11	2129111	2141238	7.774932	IGF2	Proliferation [87]
Area3	chr11	2608327	2699994	7.774932	KCNQ1OT1	Transcription [88]
Area3	chr11	2134133	2134209	7.774932	MIR483	Transcription [89]
Area3	chr9	127447673	127451405	3.212283	RPL12	Ribosome biogenesis, protein translation
Area3	chr19	49487553	49492308	3.051258	RPL13A	Ribosome biogenesis, protein translation
Area3	chr19	48615327	48619536	3.174325	RPL18	Ribosome biogenesis, protein translation
Area3	chr1	6181268	6209389	3.792397	RPL22	Ribosome biogenesis, protein translation
Area3	chr17	74203581	74210655	3.363835	RPL38	Ribosome biogenesis, protein translation
Area3	chr11	809646	812880	3.117378	RPLP2	Ribosome biogenesis, protein translation
Area3	chr19	49496364	49499689	3.051258	RPS11	Ribosome biogenesis, protein translation
Area3	chr19	39433206	39435948	3.408557	RPS16	Ribosome biogenesis, protein translation
Area3	chr16	1962051	1964860	3.301972	RPS2	Ribosome biogenesis, protein translation
Area3	chr19	8321157	8323340	3.044231	RPS28	Ribosome biogenesis, protein translation
Area3	chr17	76557765	76565348	3.374444	SNHG16	Transcription [90]
Area3	chr16	1962333	1962466	3.301972	SNORA10	Maturation of ribosomal RNA
Area3	chr2	30187433	30187566	3.83836	SNORA10B	Maturation of ribosomal RNA
Area3	chr9	136726104	136726234	3.830137	SNORA17B	Maturation of ribosomal RNA
Area3	chrY	16138247	16138379	3.968437	SNORA20	Maturation of ribosomal RNA
Area3	chr16	1965183	1965310	3.301972	SNORA78	Maturation of ribosomal RNA
Area3	chr19	10109756	10109835	5.45924	SNORD105B	Ribosomal RNA modification [63]
Area3	chr19	49490614	49490699	3.051258	SNORD33	Ribosomal RNA modification
Area3	chr14	21397291	21397401	3.835309	SNORD8	Ribosomal RNA modification
Area3	chr14	21392149	21392253	3.835309	SNORD9	Ribosomal RNA modification
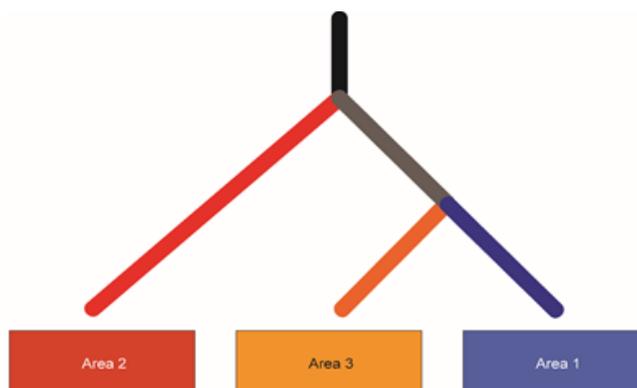
Figure 7. Phylogenetic Tree. A predicted phylogenetic tree of the tumor subclones.

4. Discussion

Despite advances in our understanding of the pathobiology of MPNST and the identification of seemingly promising therapeutic targets using a single model system in preclinical studies, no investigational agents have demonstrated efficacy following translation to human clinical trials. One element that has largely been ignored in the study of MPNST has been the possible existence of intra-tumoral heterogeneity. No single study in MPNST has focused on intra-tumoral heterogeneity. However, spatial intra-tumoral heterogeneity has become an area of interest in the study of other solid malignancies to begin to understand clonal evolution [91–95]. Within the NF1 field, researchers are beginning to appreciate the importance of understanding spatial and temporal heterogeneity. For example, Peacock et al. performed a genomic analysis of serial samples from one patient who developed an MPNST. Samples were taken at four timepoints (benign plexiform neurofibroma, MPNST pre-treatment, MPNST post-treatment, and MPNST at time of metastasis) [96]. They observed early hemizygous microdeletions in *NF1* and *TP53* with progressive amplifications of *MET*, *HGF*, and *EGFR,* highlighting the potential role of these pathways in progression. Additionally, Carrió et al. have started to examine intra-tumoral heterogeneity in PNF (plexiform neurofibromas), ANF (atypical neurofibroma) and ANNUBP (atypical neurofibromatous neoplasms with uncertain biological potential), the precursors to MPNST. They performed SNP-array analysis and exome sequencing on multiple biopsies of eight PNF, of which some had areas consistent with ANF or ANNUBP. Their data suggested that loss of a single copy of *CDKN2A/B* in *NF1* null cells is sufficient to start ANF development and that total inactivation of both copies is necessary to form ANNUBP [97]. Our study represents the first look at spatial intra-tumoral heterogeneity within an MPNST. We have demonstrated differing mutational profiles, copy number alteration signatures, and gene expression profiles within the three areas sampled. The differing mutation profile includes a variety of single nucleotide variants, including missense, frameshift, and synonymous variants. The role of synonymous variants in the tumorigenesis of MPNST is uncertain. However, there is increasing evidence that synonymous variants can alter gene expression and protein function and thus cannot be simply disregarded [98–101]. Additionally, several of the genes in Table 3a,b have previously been implicated in cancer [102–115]. For example, in Area 2, *CSK* was found to have a frameshift variant in its functional domain. *CSK* encodes a C-terminal Src kinase that has previously been found to act as a tumor suppressor in both breast cancer and prostate cancer [112–114]. Interestingly, in the context of breast cancer, Smith et al. showed that C-terminal Src kinase loss facilitated tumorigenesis by altering expression of the *PRC2* complex subunits, *EZH2* and *SUZ12* [113]. Based on these data, it is possible that alterations in *CSK* could be another way in which the *PRC2* complex is affected in MPNST. Another gene, *CCL16*, is involved in chemotaxis of human monocytes and lymphocytes. This chemokine was shown to delay mammary tumor growth and reduce rates of metastasis in mouse models [115], raising the possibility of decreased immune surveillance of our patient's MPNST secondary to a non-functional *CCL16*. In addition to the differences in single nucleotide variants, there were differences in copy number alterations across the three areas with Area

2 showing the most distinct signature in terms of copy number gains and losses. The degree to which each somatic variant, differentially expressed gene, and copy number aberration contributes to the biologic heterogeneity of the tumor remains uncertain. However, future work in our lab will be geared at elucidating this information. Finally, there was a distinct difference in gene expression among the three areas with gene ontology studies pointing toward differences in translation and protein targeting.

Taken together, these data point toward the existence of intra-tumoral heterogeneity and suggest that further investigation into this phenomenon is warranted. Additionally, these data suggest that there should be some caution taken in interpreting sequencing that comes from a single biopsy site. The advent of single cell sequencing has allowed for more rigorous evaluation of intra-tumoral heterogeneity in other cancers including acute leukemias [116,117], as well as in some solid malignancies [118,119]. Future work will be geared at using this data as the foundation to better understand clonal heterogeneity along with single cell sequencing to comprehensively evaluate intra-tumoral heterogeneity and clonal evolution of MPNST.

5. Conclusions

Significant intra-tumoral heterogeneity exists and may be a barrier to our ability to improve outcomes in patients with NF1-MPNST. These data suggest that multi-regional sampling may be necessary to understand clonal evolution, and for driver gene identification and biomarker development in the future.

References

1. Eilber, F.C.; Brennan, M.F.; Eilber, F.R.; Dry, S.M.; Singer, S.; Kattan, M.W. Validation of the Postoperative Nomogram for 12-Year Sarcoma-Specific Mortality. *Cancer* **2004**, *101*, 2270–2275. [CrossRef] [PubMed]
2. Ng, V.Y.; Scharschmidt, T.J.; Mayerson, J.L.; Fisher, J.L. Incidence and Survival in Sarcoma in the United States: A Focus on Musculoskeletal Lesions. *Anticancer Res.* **2013**, *33*, 2597–2604. [PubMed]
3. Evans, D.G.R.; Baser, M.E.; McGaughran, J.; Sharif, S.; Howard, E.; Moran, A. Malignant peripheral nerve sheath tumours in neurofibromatosis 1. *J. Med. Genet.* **2002**, *39*, 311–314. [CrossRef] [PubMed]
4. Ducatman, B.S.; Scheithauer, B.W.; Piepgras, D.G.; Reiman, H.M.; Ilstrup, D.M. Malignant Peripheral Nerve Sheath Tumors. A Clinicopathologic Study of 120 Cases. *Cancer* **1986**, *57*, 2006–2021. [CrossRef]
5. Porter, D.E.; Prasad, V.; Foster, L.; Dall, G.F.; Birch, R.; Grimer, R.J. Survival in malignant peripheral nerve sheath tumours: A comparison between sporadic and neurofibromatosis type 1-associated tumours. *Sarcoma* **2009**, *2009*, 1–5. [CrossRef]
6. Zou, C.; Smith, K.D.; Liu, J.; Lahat, G.; Myers, S.; Wang, W.L.; Zhang, W.; McCutcheon, I.E.; Slopis, J.M.; Lazar, A.J.; et al. Clinical, pathological, and molecular variables predictive of malignant peripheral nerve sheath tumor outcome. *Ann. Surg.* **2009**, *249*, 1014–1022. [CrossRef]
7. LaFemina, J.; Qin, L.X.; Moraco, N.H.; Antonescu, C.R.; Fields, R.C.; Crago, A.M.; Brennan, M.F.; Singer, S. Oncologic outcomes of sporadic, neurofibromatosis-associated, and radiation-induced malignant peripheral nerve sheath tumors. *Ann. Surg. Oncol.* **2013**, *20*, 66–72. [CrossRef]
8. Farid, M.; Demicco, E.G.; Garcia, R.; Ahn, L.; Merola, P.R.; Cioffi, A.; Maki, R.G. Malignant Peripheral Nerve Sheath Tumors. *Oncologist* **2014**, *19*, 193–201. [CrossRef]

9. Anghileri, M.; Miceli, R.; Fiore, M.; Mariani, L.; Ferrari, A.; Mussi, C.; Lozza, L.; Collini, P.; Olmi, P.; Casali, P.G.; et al. Malignant Peripheral Nerve Sheath Tumors: Prognostic Factors and Survival in a Series of Patients Treated at a Single Institution. *Cancer* **2006**, *107*, 1065–1074. [CrossRef]

10. Stucky, C.C.; Johnson, K.N.; Gray, R.J.; Pockaj, B.A.; Ocal, I.T.; Rose, P.S.; Wasif, N. Malignant peripheral nerve sheath tumors (MPNST): The Mayo Clinic experience. *Ann. Surg. Oncol.* **2012**, *19*, 878–885. [CrossRef]

11. Ferner, R.E.; Gutmann, D.H. International Consensus Statement on Malignant Peripheral Nerve Sheath Tumors in Neurofibromatosis. *Cancer Res.* **2002**, *62*, 1573–1577.

12. Kroep, J.R.; Ouali, M.; Gelderblom, H.; Le Cesne, A.; Dekker, T.J.; Van Glabbeke, M.; Hogendoorn, P.C.; Hohenberger, P. First-Line Chemotherapy for Malignant Peripheral Nerve Sheath Tumor (MPNST) versus Other Histological Soft Tissue Sarcoma Subtypes and as a Prognostic Factor for MPNST: An EORTC Soft Tissue and Bone Sarcoma Group Study. *Ann. Oncol.* **2011**, *22*, 207–214. [CrossRef] [PubMed]

13. James, A.W.; Shurell, E.; Singh, A.; Dry, S.M.; Eilber, F.C. Malignant Peripheral Nerve Sheath Tumor. *Surg. Oncol. Clin. N. Am.* **2016**, *25*, 789–802. [CrossRef] [PubMed]

14. Cichowski, K.; Shih, T.S.; Schmitt, E.; Santiago, S.; Reilly, K.; McLaughlin, M.E.; Bronson, R.T.; Jacks, T. Mouse Models of Tumor Development in Neurofibromatosis Type 1. *Science* **1999**, *286*, 2172–2176. [CrossRef] [PubMed]

15. Vogel, K.S.; Klesse, L.J.; Velasco-Miguel, S.; Meyers, K.; Rushing, E.J.; Parada, L.F. Mouse Tumor Model for Neurofibromatosis Type 1. *Science* **1999**, *286*, 2176–2179. [CrossRef]

16. Bradtmoller, M.; Hartmann, C.; Zietsch, J.; Jäschke, S.; Mautner, V.F.; Kurtz, A.; Park, S.J.; Baier, M.; Harder, A.; Reuss, D.; et al. Impaired Pten Expression in Human Malignant Peripheral Nerve Sheath Tumours. *PLoS ONE* **2012**. [CrossRef]

17. Keng, V.W.; Rahrmann, E.P.; Watson, A.L.; Tschida, B.R.; Moertel, C.L.; Jessen, W.J.; Rizvi, T.A.; Collins, M.H.; Ratner, N.; Largaespada, D.A. PTEN and NF1 inactivation in Schwann cells produces a severe phenotype in the peripheral nervous system that promotes the development and malignant progression of peripheral nerve sheath tumors. *Cancer Res.* **2012**, *72*, 3405–3413. [CrossRef]

18. Gregorian, C.; Nakashima, J.; Dry, S.M.; Nghiemphu, P.L.; Smith, K.B.; Ao, Y.; Dang, J.; Lawson, G.; Mellinghoff, I.K.; Mischel, P.S.; et al. PTEN dosage is essential for neurofibroma development and malignant transformation. *Proc. Natl. Acad. Sci. USA* **2009**, *106*, 19479–19484. [CrossRef]

19. Kourea, H.P.; Orlow, I.; Scheithauer, B.W.; Cordon-Cardo, C.; Woodruff, J.M. Deletions of the INK4A gene occur in malignant peripheral nerve sheath tumors but not in neurofibromas. *Am. J. Path.* **1999**, *155*, 1855–1860. [CrossRef]

20. Lu, H.C.; Eulo, V.; Apicelli, A.J.; Pekmezci, M.; Tao, Y.; Luo, J.; Hirbe, A.C.; Dahiya, S. Aberrant ATRX protein expression is associated with poor overall survival in NF1-MPNST. *Oncotarget* **2018**, *9*, 23018–23028. [CrossRef]

21. Lee, W.; Teckie, S.; Wiesner, T.; Ran, L.; Prieto Granada, C.N.; Lin, M.; Zhu, S.; Cao, Z.; Liang, Y.; Sboner, A.; et al. PRC2 is recurrently inactivated through EED or SUZ12 loss in malignant peripheral nerve sheath tumors. *Nat. Genet.* **2014**, *46*, 1227–1232. [CrossRef] [PubMed]

22. Holtkamp, N.; Okuducu, A.F.; Mucha, J.; Afanasieva, A.; Hartmann, C.; Atallah, I.; Estevez-Schwarz, L.; Mawrin, C.; Friedrich, R.E.; Mautner, V.F.; et al. Mutation and expression of PDGFRA and KIT in malignant peripheral nerve sheath tumors, and its implications for imatinib sensitivity. *Carcinogenesis* **2006**, *27*, 664–671. [CrossRef] [PubMed]

23. DeClue, J.E.; Heffelfinger, S.; Benvenuto, G.; Ling, B.; Li, S.; Rui, W.; Vass, W.C.; Viskochil, D.; Ratner, N. Epidermal growth factor receptor expression in neurofibromatosis type 1-related tumors and NF1 animal models. *J. Clin. Investig.* **2000**, *105*, 1233–1241. [CrossRef] [PubMed]

24. Yang, J.; Ylipää, A.; Sun, Y.; Zheng, H.; Chen, K.; Nykter, M.; Trent, J.; Ratner, N.; Lev, D.C.; Zhang, W. Genomic and molecular characterization of malignant peripheral nerve sheath tumor identifies the IGF1R pathway as a primary target for treatment. *Clin. Cancer Res.* **2011**, *17*, 7563–7573. [CrossRef]

25. Symposium on Linkage of von Recklinghausen Neurofibromatosis (NF1). Closing in on the gene for von Recklinghausen neurofibromatosis. *Genomics* **1987**, *1*, 335–383.

26. Talevich, E.; Shain, A.H.; Botton, T.; Bastian, B.C. CNVkit: Genome-Wide Copy Number Detection and Visualization from Targeted DNA Sequencing. *PLoS Comput. Biol.* **2016**, *12*, e1004873. [CrossRef]

27. Li, H. Aligning sequence reads, clone sequences and assembly contigs with BWA-MEM. *arXiv Preprint* **2013**, arXiv:1303.3997.

28. Chen, X.; Schulz-Trieglaff, O.; Shaw, R.; Barnes, B.; Schlesinger, F.; Källberg, M.; Cox, A.J.; Kruglyak, S.; Saunders, C.T. Manta: Rapid detection of structural variants and indels for germline and cancer sequencing applications. *Bioinformatics* **2015**, *32*, 1220–1222. [CrossRef]

29. Koboldt, D.C.; Zhang, Q.; Larson, D.E.; Shen, D.; McLellan, M.D.; Lin, L.; Miller, C.A.; Mardis, E.R.; Ding, L.; Wilson, R.K. VarScan 2: Somatic mutation and copy number alteration discovery in cancer by exome sequencing. *Genome Res.* **2012**, *22*, 568–576. [CrossRef]

30. Kim, S.; Scheffler, K.; Halpern, A.L.; Bekritsky, M.A.; Noh, E.; Källberg, M.; Chen, X.; Kim, Y.; Beyter, D.; Krusche, P.; et al. Strelka2: Fast and accurate calling of germline and somatic variants. *Nat. Methods* **2018**, *15*, 591–594. [CrossRef]

31. Cibulskis, K.; Lawrence, M.S.; Carter, S.L.; Sivachenko, A.; Jaffe, D.; Sougnez, C.; Gabriel, S.; Meyerson, M.; Lander, E.S.; Getz, G. Sensitive detection of somatic point mutations in impure and heterogeneous cancer samples. *Nat. Biotechnol.* **2013**, *31*, 213–219. [CrossRef] [PubMed]

32. Ye, K.; Schulz, M.H.; Long, Q.; Apweiler, R.; Ning, Z. Pindel: A pattern growth approach to detect break points of large deletions and medium sized insertions from paired-end short reads. *Bioinformatics (Oxford, England)* **2009**, *25*, 2865–2871. [CrossRef] [PubMed]

33. McLaren, W.; Gil, L.; Hunt, S.E.; Riat, H.S.; Ritchie, G.R.; Thormann, A.; Flicek, P.; Cunningham, F. The Ensembl Variant Effect Predictor. *Genome Biol.* **2016**, *17*. [CrossRef] [PubMed]

34. Bioconductor: Genomic Visualizations in R. Available online: https://bioconductor.org/packages/release/bioc/html/GenVisR.html (accessed on 24 February 2020).

35. Bamford, S.; Dawson, E.; Forbes, S.; Clements, J.; Pettett, R.; Dogan, A.; Flanagan, A.; Teague, J.; Futreal, P.A.; Stratton, M.R.; et al. The COSMIC (Catalogue of Somatic Mutations in Cancer) database and website. *Br. J. Cancer* **2004**, *91*, 355–358. [CrossRef]

36. Landrum, M.J.; Lee, J.M.; Benson, M.; Brown, G.; Chao, C.; Chitipiralla, S.; Gu, B.; Hart, J.; Hoffman, D.; Hoover, J.; et al. ClinVar: Public archive of interpretations of clinically relevant variants. *Nucleic Acids Res.* **2016**, *44*, 862–868. [CrossRef]

37. Pauline, C.; Ng, S.H. SIFT: Predicting amino acid changes that affect protein function. *Nucleic Acids Res.* **2003**, *31*, 3812–3814.

38. Adzhubei, I.A.; Schmidt, S.; Peshkin, L.; Ramensky, V.E.; Gerasimova, A.; Bork, P.; Kondrashov, A.S.; Sunyaev, S.R. A method and server for predicting damaging missense mutations. *Nat Methods* **2010**, *7*, 248–249. [CrossRef]

39. Miller, C.A.; White, B.S.; Dees, N.D.; Griffith, M.; Welch, J.S.; Griffith, O.L.; Vij, R.; Tomasson, M.H.; Graubert, T.A.; Walter, M.J.; et al. SciClone: Inferring clonal architecture and tracking the spatial and temporal patterns of tumor evolution. *PLoS Comput. Biol.* **2014**. [CrossRef]

40. Dang, H.X.; White, B.S.; Foltz, S.M.; Miller, C.A.; Luo, J.; Fields, R.C.; Maher, C.A. ClonEvol: Clonal ordering and visualization in cancer sequencing. *Ann. Oncol.* **2017**, *28*, 3076–3082. [CrossRef]

41. Xing, Y.; Yu, T.; Wu, Y.N.; Roy, M.; Kim, J.; Lee, C. An expectation-maximization algorithm for probabilistic reconstructions of full-length isoforms from splice graphs. *Nucleic Acids Res.* **2006**, *34*, 3150–3160. [CrossRef]

42. Robinson, M.D.; McCarthy, D.J.; Smyth, G.K. edgeR: A Bioconductor package for differential expression analysis of digital gene expression data. *Bioinformatics* **2010**, *26*, 139–140. [CrossRef] [PubMed]

43. Warnes, G.R.; Bolker, B.; Bonebakker, L.; Gentleman, R.; Huber, W.; Liaw, A.; Lumley, T.; Maechler, M.; Magnusson, A.; Moeller, S.; et al. gplots: Various R Programming Tools for Plotting Data. Seattle, WA, USA, 2015. Available online: https://www.scienceopen.com/document?vid=0e5d8e31-1fe4-492f-a3d8-8cd71b2b8ad9 (accessed on 29 April 2020).

44. Partek Flow Documentation: Gene-specific Analysis. Available online: https://documentation.partek.com/display/FLOWDOC/Gene-specific+Analysis (accessed on 24 February 2020).

45. Thomas, P.D.; Campbell, M.J.; Kejariwal, A.; Mi, H.; Karlak, B.; Daverman, R.; Diemer, K.; Muruganujan, A.; Narechania, A. PANTHER: A library of protein families and subfamilies indexed by function. *Genome Res.* **2003**, *13*, 2129–2141. [CrossRef] [PubMed]

46. Guillou, L.; Coindre, J.M.; Bonichon, F.; Nguyen, B.B.; Terrier, P.; Collin, F.; Vilain, M.O.; Mandard, A.M.; Le Doussal, V.; Leroux, A.; et al. Comparative study of the National Cancer Institute and French Federation of Cancer Centers Sarcoma Group grading systems in a population of 410 adult patients with soft tissue sarcoma. *J. Clin. Oncol.* **1997**, *15*, 350–362. [CrossRef] [PubMed]

47. Gao, J.; Aksoy, B.A.; Dogrusoz, U.; Dresdner, G.; Gross, B.; Sumer, S.O.; Sun, Y.; Jacobsen, A.; Sinha, R.; Larsson, E.; et al. Integrative analysis of complex cancer genomics and clinical profiles using the cBioPortal. *Sci. Signal* **2013**. [CrossRef]

48. Wang, T.; Wang, H.; Yang, S.; Guo, H.; Zhang, B.; Guo, H.; Wang, L.; Zhu, G.; Zhang, Y.; Zhou, H.; et al. Association of APEX1 and OGG1 gene polymorphisms with breast cancer risk among Han women in the Gansu Province of China. *BMC Med. Genet.* **2018**, *19*, 67. [CrossRef]

49. Kim, H.B.; Lim, H.J.; Lee, H.J.; Park, J.H.; Park, S.G. Evaluation and Clinical Significance of Jagged-1-activated Notch Signaling by APEX1 in Colorectal Cancer. *Anticancer Res.* **2019**, *39*, 6097–6105. [CrossRef]

50. Kim, H.B.; Cho, W.J.; Choi, N.G.; Kim, S.S.; Park, J.H.; Lee, H.J.; Park, S.G. Clinical implications of APEX1 and Jagged1 as chemoresistance factors in biliary tract cancer. *Ann. Surg. Treat. Res.* **2017**, *92*, 15–22. [CrossRef]

51. Blazquez, L.; Emmett, W.; Faraway, R.; Pineda, J.M.B.; Bajew, S.; Gohr, A.; Haberman, N.; Sibley, C.R.; Bradley, R.K.; Irimia, M.; et al. Exon Junction Complex Shapes the Transcriptome by Repressing Recursive Splicing. *Mol. Cell* **2018**, *72*, 496–509. [CrossRef]

52. Shen, Y.N.; Bae, I.S.; Park, G.H.; Choi, H.S.; Lee, K.H.; Kim, S.H. MicroRNA-196b enhances the radiosensitivity of SNU-638 gastric cancer cells by targeting RAD23B. *Biomed. Pharmacother.* **2018**, *105*, 362–369. [CrossRef]

53. Linge, A.; Maurya, P.; Friedrich, K.; Baretton, G.B.; Kelly, S.; Henry, M.; Clynes, M.; Larkin, A.; Meleady, P. Identification and functional validation of RAD23B as a potential protein in human breast cancer progression. *J. Proteome Res.* **2014**, *13*, 3212–3222. [CrossRef]

54. Luo, C.; Cheng, Y.; Liu, Y.; Chen, L.; Liu, L.; Wei, N.; Xie, Z.; Wu, W.; Feng, Y. SRSF2 Regulates Alternative Splicing to Drive Hepatocellular Carcinoma Development. *Cancer Res.* **2017**, *77*, 1168–1178. [CrossRef] [PubMed]

55. Liang, Y.; Tebaldi, T.; Rejeski, K.; Joshi, P.; Stefani, G.; Taylor, A.; Song, Y.; Vasic, R.; Maziarz, J.; Balasubramanian, K. SRSF2 mutations drive oncogenesis by activating a global program of aberrant alternative splicing in hematopoietic cells. *Leukemia* **2018**, *32*, 2659–2671. [CrossRef] [PubMed]

56. Gu, L.; Lu, L.; Zhou, D.; Liu, Z. Long Noncoding RNA BCYRN1 Promotes the Proliferation of Colorectal Cancer Cells via Up-Regulating NPR3 Expression. *Cell Physiol. Biochem.* **2018**, *48*, 2337–2349. [CrossRef]

57. Li, X.; Li, J.; Li, F. P21 activated kinase 4 binds translation elongation factor eEF1A1 to promote gastric cancer cell migration and invasion. *Oncol. Rep.* **2017**, *37*, 2857–2864. [CrossRef]

58. Shi, N.; Chen, X.; Liu, R.; Wang, D.; Su, M.; Wang, Q.; He, A.; Gu, H. Eukaryotic elongation factors 2 promotes tumor cell proliferation and correlates with poor prognosis in ovarian cancer. *Tissue Cell* **2018**, *53*, 53–60. [CrossRef] [PubMed]

59. Wang, H.; He, Z.; Xia, L.; Zhang, W.; Xu, L.; Yue, X.; Ru, X.; Xu, Y. PSMB4 overexpression enhances the cell growth and viability of breast cancer cells leading to a poor prognosis. *Oncol. Rep.* **2018**, *40*, 2343–2352. [CrossRef]

60. Liu, R.; Lu, S.; Deng, Y.; Yang, S.; He, S.; Cai, J.; Qiang, F.; Chen, C.; Zhang, W.; Zhao, S.; et al. PSMB4 expression associates with epithelial ovarian cancer growth and poor prognosis. *Arch. Gynecol. Obstet.* **2016**, *293*, 1297–1307. [CrossRef]

61. Xu, X.; Xiong, X.; Sun, Y. The role of ribosomal proteins in the regulation of cell proliferation, tumorigenesis, and genomic integrity. *Sci. China Life Sci.* **2016**, *59*, 656–672. [CrossRef]

62. Nallar, S.C.; Kalvakolanu, D.V. Regulation of snoRNAs in Cancer: Close Encounters with Interferon. *J. Interferon Cytokine Res.* **2013**, *33*, 189–198. [CrossRef]

63. Falaleeva, M.; Welden, J.R.; Duncan, M.J.; Stamm, S. C/D-box snoRNAs form methylating and non-methylating ribonucleoprotein complexes: Old dogs show new tricks. *Bioessays* **2017**, *39*. [CrossRef]

64. Dong, X.; Han, Y.; Sun, Z.; Xu, J. Actin γ 1, a new skin cancer pathogenic gene, identified by the biological feature-based classification. *J. Cell Biochem.* **2018**, *119*, 1406–1419. [CrossRef] [PubMed]

65. Luo, Y.; Kong, F.; Wang, Z.; Chen, D.; Liu, Q.; Wang, T.; Xu, R.; Wang, X.; Yang, J.Y. Loss of ASAP3 destabilizes cytoskeletal protein ACTG1 to suppress cancer cell migration. *Mol. Med. Rep.* **2014**, *9*, 387–394. [CrossRef] [PubMed]

66. Munschauer, M.; Nguyen, C.T.; Sirokman, K.; Hartigan, C.R.; Hogstrom, L.; Engreitz, J.M.; Ulirsch, J.C.; Fulco, C.P.; Subramanian, V.; Chen, J.; et al. The NORAD lncRNA assembles a topoisomerase complex critical for genome stability. *Nature* **2018**, *561*, 132–136. [CrossRef] [PubMed]

67. Liang, L.; Li, Q.; Huang, L.Y.; Li, D.W.; Wang, Y.W.; Li, X.X.; Cai, S.J. Loss of ARHGDIA expression is associated with poor prognosis in HCC and promotes invasion and metastasis of HCC cells. *Int. J. Oncol.* **2014**, *45*, 659–666. [CrossRef] [PubMed]

68. Riihilä, P.; Viiklepp, K.; Nissinen, L.; Farshchian, M.; Kallajoki, M.; Kivisaari, A.; Meri, S.; Peltonen, J.; Peltonen, S.; Kähäri, V.M. Tumour-cell-derived complement components C1r and C1s promote growth of cutaneous squamous cell carcinoma. *Br. J. Dermatol.* **2020**, *182*, 658–670. [CrossRef] [PubMed]

69. Wheeler, L.J.; Watson, Z.L.; Qamar, L.; Yamamoto, T.M.; Post, M.D.; Berning, A.A.; Spillman, M.A.; Behbakht, K.; Bitler, B.G. CBX2 identified as driver of anoikis escape and dissemination in high grade serous ovarian cancer. *Oncogenesis* **2018**, *7*, 92. [CrossRef]

70. Liu, J.; Shen, J.X.; Wu, H.T.; Li, X.L.; Wen, X.F.; Du, C.W.; Zhang, G.J. Collagen 1A1 (COL1A1) promotes metastasis of breast cancer and is a potential therapeutic target. *Discov. Med.* **2018**, *25*, 211–223.

71. Menendez, J.A.; Lupu, R. Fatty acid synthase and the lipogenic phenotype in cancer pathogenesis. *Nat. Rev. Cancer* **2007**, *7*, 763–777. [CrossRef]

72. Kamil, M.; Shinsato, Y.; Higa, N.; Hirano, T.; Idogawa, M.; Takajo, T.; Minami, K.; Shimokawa, M.; Yamamoto, M.; Kawahara, K.; et al. High filamin-C expression predicts enhanced invasiveness and poor outcome in glioblastoma multiforme. *Br. J. Cancer* **2019**, *120*, 819–826. [CrossRef]

73. Zhu, Y.; Kakinuma, N.; Wang, Y.; Kiyama, R. Kank proteins: A new family of ankyrin-repeat domain-containing proteins. *Biochim. Biophys. Act* **2008**, *1780*, 128–133. [CrossRef]

74. Trussart, C.; Pirlot, C.; Di Valentin, E.; Piette, J.; Habraken, Y. Melanoma antigen-D2 controls cell cycle progression and modulates the DNA damage response. *Biochem. Pharmacol.* **2018**, *153*, 217–229. [CrossRef] [PubMed]

75. Wang, P.C.; Hu, Z.Q.; Zhou, S.L.; Zhan, H.; Zhou, Z.J.; Luo, C.B.; Huang, X.W. Downregulation of MAGE family member H1 enhances hepatocellular carcinoma progression and serves as a biomarker for patient prognosis. *Future Oncol.* **2018**, *14*, 1177–1186. [CrossRef] [PubMed]

76. Qu, K.; Wang, Z.; Fan, H.; Li, J.; Liu, J.; Li, P.; Liang, Z.; An, H.; Jiang, Y.; Lin, Q.; et al. MCM7 promotes cancer progression through cyclin D1-dependent signaling and serves as a prognostic marker for patients with hepatocellular carcinoma. *Cell Death Dis* **2017**, *8*, e2603. [CrossRef] [PubMed]

77. Nguyen, A.T.; Chia, J.; Ros, M.; Hui, K.M.; Saltel, F.; Bard, F. Organelle Specific O-Glycosylation Drives MMP14 Activation, Tumor Growth, and Metastasis. *Cancer Cell* **2017**, *32*, 639–653. [CrossRef]

78. Hu, G.; Zhang, J.; Xu, F.; Deng, H.; Zhang, W.; Kang, S.; Liang, W. Stomatin-like protein 2 inhibits cisplatin-induced apoptosis through MEK/ERK signaling and the mitochondrial apoptosis pathway in cervical cancer cells. *Cancer Sci.* **2018**, *109*, 1357–1368. [CrossRef]

79. Du, W.L.; Fang, Q.; Chen, Y.; Teng, J.W.; Xiao, Y.S.; Xie, P.; Jin, B.; Wang, J.Q. Effect of silencing the T-Box transcription factor TBX2 in prostate cancer PC3 and LNCaP cells. *Mol. Med. Rep.* **2017**, *16*, 6050–6058. [CrossRef]

80. Czerwińska, P.; Mazurek, S.; Wiznerowicz, M. The complexity of TRIM28 contribution to cancer. *J. Biomed. Sci.* **2017**, *29*, 63. [CrossRef]

81. Lan, B.; Chai, S.; Wang, P.; Wang, K. VCP/p97/Cdc48, A Linking of Protein Homeostasis and Cancer Therapy. *Curr. Mol. Med.* **2017**, *17*, 608–618. [CrossRef]

82. Hwang, W.; Chiu, Y.F.; Kuo, M.H.; Lee, K.L.; Lee, A.C.; Yu, C.C.; Chang, J.L.; Huang, W.C.; Hsiao, S.H.; Lin, S.E.; et al. Expression of Neuroendocrine Factor VGF in Lung Cancer Cells Confers Resistance to EGFR Kinase Inhibitors and Triggers Epithelial-to-Mesenchymal Transition. *Cancer Res.* **2017**, *77*, 3013–3026. [CrossRef]

83. De Blasio, A.; Vento, R.; Di Fiore, R. Mcl-1 targeting could be an intriguing perspective to cure cancer. *J. Cell Physiol.* **2018**, *233*, 8482–8498. [CrossRef]

84. Louie, S.M.; Grossman, E.A.; Crawford, L.A.; Ding, L.; Camarda, R.; Huffman, T.R.; Miyamoto, D.K.; Goga, A.; Weerapana, E.; Nomura, D.K. GSTP1 Is a Driver of Triple-Negative Breast Cancer Cell Metabolism and Pathogenicity. *Cell Chem. Biol.* **2016**, *23*, 567–578. [CrossRef] [PubMed]

85. Bianchi, M.; Crinelli, R.; Giacomini, E.; Carloni, E.; Radici, L.; Scarpa, E.S.; Tasini, F.; Magnani, M. A negative feedback mechanism links UBC gene expression to ubiquitin levels by affecting RNA splicing rather than transcription. *Sci. Rep.* **2019**, *9*, 18556. [CrossRef] [PubMed]

86. Lin, L.; Li, X.; Pan, C.; Lin, W.; Shao, R.; Liu, Y.; Zhang, J.; Luo, Y.; Qian, K.; Shi, M.; et al. ATXN2L upregulated by epidermal growth factor promotes gastric cancer cell invasiveness and oxaliplatin resistance. *Cell Death Dis.* **2019**, *10*, 173. [CrossRef] [PubMed]

87. Livingstone, C. IGF2 and cancer. *Endocr. Relat. Cancer* **2013**, *20*, 321–339. [CrossRef] [PubMed]

88. Feng, W.; Wang, C.; Liang, C.; Yang, H.; Chen, D.; Yu, X.; Zhao, W.; Geng, D.; Li, S.; Chen, Z.; et al. The Dysregulated Expression of KCNQ1OT1 and Its Interaction with Downstream Factors miR-145/CCNE2 in Breast Cancer Cells. *Cell Physiol. Biochem.* **2018**, *49*, 432–446. [CrossRef]

89. Zhang, Y.; Hu, J.F.; Wang, H.; Cui, J.; Gao, S.; Hoffman, A.R.; Li, W. CRISPR Cas9-guided chromatin immunoprecipitation identifies miR483 as an epigenetic modulator of IGF2 imprinting in tumors. *Oncotarget* **2017**, *8*, 34177–34190. [CrossRef]

90. Gong, C.Y.; Tang, R.; Nan, W.; Zhou, K.S.; Zhang, H.H. Role of SNHG16 in human cancer. *Clin. Chim. Acta* **2020**, *503*, 175–180. [CrossRef]

91. Gerlinger, M.; Horswell, S.; Larkin, J.; Rowan, A.J.; Salm, M.P.; Varela, I.; Fisher, R.; McGranahan, N.; Matthews, N.; Santos, C.R.; et al. Genomic architecture and evolution of clear cell renal cell carcinomas defined by multiregion sequencing. *Nat. Genet.* **2014**, *46*, 225–233. [CrossRef]

92. Yates, L.R.; Gerstung, M.; Knappskog, S.; Desmedt, C.; Gundem, G.; Van Loo, P.; Aas, T.; Alexandrov, L.B.; Larsimont, D.; Davies, H.; et al. Subclonal diversification of primary breast cancer revealed by multiregion sequencing. *Nat. Med.* **2015**, *21*, 751–759. [CrossRef]

93. Hao, J.J.; Lin, D.C.; Dinh, H.Q.; Mayakonda, A.; Jiang, Y.Y.; Chang, C.; Jiang, Y.; Lu, C.C.; Shi, Z.Z.; Xu, X.; et al. Spatial intratumoral heterogeneity and temporal clonal evolution in esophageal squamous cell carcinoma. *Nat. Genet.* **2016**, *48*, 1500–1507. [CrossRef]

94. Jamal-Hanjani, M.; Wilson, G.A.; McGranahan, N.; Birkbak, N.J.; Watkins, T.B.K.; Veeriah, S.; Shafi, S.; Johnson, D.H.; Mitter, R.; Rosenthal, R.; et al. Tracking the evolution of non-small-cell lung cancer. *N. Engl. J. Med.* **2017**, *376*, 2109–2121. [CrossRef] [PubMed]

95. Harbst, K.; Lauss, M.; Cirenajwis, H.; Isaksson, K.; Rosengren, F.; Törngren, T.; Kvist, A.; Johansson, M.C.; Vallon-Christersson, J.; Baldetorp, B.; et al. Multiregion whole-exome sequencing uncovers the genetic evolution and mutational heterogeneity of early-stage metastatic melanoma. *Cancer Res.* **2016**, *76*, 4765–4774. [CrossRef] [PubMed]

96. Peacock, J.D.; Pridgeon, M.G.; Tovar, E.A.; Essenburg, C.J.; Bowman, M.; Madaj, Z.; Koeman, J.; Boguslawski, E.A.; Grit, J.; Dodd, R.D.; et al. Genomic Status of MET Potentiates Sensitivity to MET and MEK Inhibition in NF1-Related Malignant Peripheral Nerve Sheath Tumors. *Cancer Res.* **2018**, *78*, 3672–3678. [CrossRef] [PubMed]

97. Carrió, M.; Gel, B.; Terribas, E.; Zucchiatti, A.C.; Moliné, T.; Rosas, I.; Teulé, Á.; Ramón, Y.; Cajal, S.; López-Gutiérrez, J.C.; et al. Analysis of intratumor heterogeneity in Neurofibromatosis type 1 plexiform neurofibromas and neurofibromas with atypical features: Correlating histological and genomic findings. *Hum. Mutat.* **2018**, *39*, 1112–1125. [CrossRef] [PubMed]

98. Nackley, A.G.; Shabalina, S.A.; Tchivileva, I.E.; Satterfield, K.; Korchynskyi, O.; Makarov, S.S.; Maixner, W.; Diatchenko, L. Human catechol-O-methyltransferase haplotypes modulate protein expression by altering mRNA secondary structure. *Science* **2006**, *314*, 1930–1933. [CrossRef] [PubMed]

99. Kimchi-Sarfaty, C.; Oh, J.M.; Kim, I.W.; Sauna, Z.E.; Calcagno, A.M.; Ambudkar, S.V.; Gottesman, M.M. A "silent" polymorphism in the MDR1 gene changes substrate specificity. *Science* **2007**, *315*, 525–528. [CrossRef]

100. Kudla, G.; Murray, A.W.; Tollervey, D.; Plotkin, J.B. Coding-sequence determinants of gene expression in Escherichia coli. *Science* **2009**, *324*, 255–258. [CrossRef]

101. Sauna, Z.E.; Kimchi-Sarfaty, C. Understanding the contribution of synonymous mutations to human disease. *Nat. Rev. Genet.* **2011**, *12*, 683–691. [CrossRef]

102. Pey, J.; San José-Eneriz, E.; Ochoa, M.C.; Apaolaza, I.; de Atauri, P.; Rubio, A.; Cendoya, X.; Miranda, E.; Garate, L.; Cascante, M.; et al. In-silico gene essentiality analysis of polyamine biosynthesis reveals APRT as a potential target in cancer. *Sci. Rep.* **2017**, *7*, 14358. [CrossRef]

103. Shen, L.; Ke, Q.; Chai, J.; Zhang, C.; Qiu, L.; Peng, F.; Deng, X.; Luo, Z. PAG1 promotes the inherent radioresistance of laryngeal cancer cells via activation of STAT3. *Exp. Cell Res.* **2018**, *370*, 127–136. [CrossRef]

104. Agarwal, S.; Ghosh, R.; Chen, Z.; Lakoma, A.; Gunaratne, P.H.; Kim, E.S.; Shohet, J.M. Transmembrane adaptor protein PAG1 is a novel tumor suppressor in neuroblastoma. *Oncotarget* **2016**, *7*, 24018–24026. [CrossRef] [PubMed]

105. Jiang, D.; Hu, B.; Wei, L.; Xiong, Y.; Wang, G.; Ni, T.; Zong, C.; Ni, R.; Lu, C. High expression of vacuolar protein sorting 4B (VPS4B) is associated with accelerated cell proliferation and poor prognosis in human hepatocellular carcinoma. *Pathol. Res. Pract.* **2015**, *211*, 240–247. [CrossRef] [PubMed]

106. Liu, Y.; Lv, L.; Xue, Q.; Wan, C.; Ni, T.; Chen, B.; Liu, Y.; Zhou, Y.; Ni, R.; Mao, G. Vacuolar protein sorting 4B, an ATPase protein positively regulates the progression of NSCLC via promoting cell division. *Mol. Cell Biochem.* **2013**, *381*, 163–171. [CrossRef] [PubMed]

107. Lin, H.H.; Li, X.; Chen, J.L.; Sun, X.; Cooper, F.N.; Chen, Y.R.; Zhang, W.; Chung, Y.; Li, A.; Cheng, C.T.; et al. Identification of an AAA ATPase VPS4B-dependent pathway that modulates epidermal growth factor receptor abundance and signaling during hypoxia. *Mol. Cell Biol.* **2012**, *32*, 1124–1138. [CrossRef] [PubMed]

108. Hazawa, M.; Lin, D.C.; Handral, H.; Xu, L.; Chen, Y.; Jiang, Y.Y.; Mayakonda, A.; Ding, L.W.; Meng, X.; Sharma, A.; et al. ZNF750 is a lineage-specific tumour suppressor in squamous cell carcinoma. *Oncogene* **2017**, *36*, 2243–2254. [CrossRef] [PubMed]

109. Zhang, P.; He, Q.; Lei, Y.; Li, Y.; Wen, X.; Hong, M.; Zhang, J.; Ren, X.; Wang, Y.; Yang, X.; et al. m6A-mediated ZNF750 repression facilitates nasopharyngeal carcinoma progression. *Cell Death Dis.* **2018**, *5*, 1169. [CrossRef]

110. Feng, T.; Sun, L.; Qi, W.; Pan, F.; Lv, J.; Guo, J.; Zhao, S.; Ding, A.; Qiu, W. Prognostic significance of Tspan9 in gastric cancer. *Mol. Clin. Oncol.* **2016**, *5*, 231–236. [CrossRef]

111. Qi, Y.; Lv, J.; Liu, S.; Sun, L.; Wang, Y.; Li, H.; Qi, W.; Qiu, W. TSPAN9 and EMILIN1 synergistically inhibit the migration and invasion of gastric cancer cells by increasing TSPAN9 expression. *BMC Cancer* **2019**, *19*, 630. [CrossRef]

112. Xiao, T.; Li, W.; Wang, X.; Xu, H.; Yang, J.; Wu, Q.; Huang, Y.; Geradts, J.; Jiang, P.; Fei, T.; et al. Estrogen-regulated feedback loop limits the efficacy of estrogen receptor–targeted breast cancer therapy. *Proc. Natl. Acad. Sci. USA* **2018**, *115*, 7869–7878. [CrossRef]

113. Smith, H.W.; Hirukawa, A.; Sanguin-Gendreau, V.; Nandi, I.; Dufour, C.R.; Zuo, D.; Tandoc, K.; Leibovitch, M.; Singh, S.; Rennhack, J.P.; et al. An ErbB2/c-Src axis links bioenergetics with PRC2 translation to drive epigenetic reprogramming and mammary tumorigenesis. *Nat. Commun.* **2019**, *10*. [CrossRef]

114. Yang, C.C.; Fazli, L.; Loguercio, S.; Zharkikh, I.; Aza-Blanc, P.; Gleave, M.E.; Wolf, D.A. Downregulation of c-SRC kinase CSK promotes castration resistant prostate cancer and pinpoints a novel disease subclass. *Oncotarget* **2015**, *6*, 22060–22071. [CrossRef] [PubMed]

115. Guiducci, C.; Di Carlo, E.; Parenza, M.; Hitt, M.; Giovarelli, M.; Musiani, P.; Colombo, M.P. Intralesional injection of adenovirus encoding CC chemokine ligand 16 inhibits mammary tumor growth and prevents metastatic-induced death after surgical removal of the treated primary tumor. *J. Immunol.* **2004**, *172*, 4026–4036. [CrossRef] [PubMed]

116. Paulsson, K. Genomic heterogeneity in acute leukemia. *Cytogenet. Genome Res.* **2013**, *139*, 174–180. [CrossRef] [PubMed]

117. Saadatpour, A.; Guo, G.; Orkin, S.H.; Yuan, G.C. Characterizing heterogeneity in leukemic cells using single-cell gene expression analysis. *Genome Biol.* **2014**, *15*, 525. [CrossRef]

118. Navin, N.; Kendall, J.; Troge, J.; Andrews, P.; Rodgers, L.; McIndoo, J.; Cook, K.; Stepansky, A.; Levy, D.; Esposito, D.; et al. Tumor evolution inferred by single cell sequencing. *Nature* **2011**, *472*, 90–94. [CrossRef]

119. Xu, X.; Hou, Y.; Yin, X.; Bao, L.; Tang, A.; Song, L.; Li, F.; Tsang, S.; Wu, K.; Wu, H.; et al. Single-cell exome sequencing reveals single-nucleotide mutation characteristics of a kidney tumor. *Cell* **2012**, *148*, 886–895. [CrossRef]